Journal of The
Electrochemical Society

Investigation of the Electrochemical Acetone Reduction Reaction in a PEM-Setup

To cite this article: Axel Marth *et al* 2024 *J. Electrochem. Soc.* **171** 114505

Journal of The Electrochemical Society, 2024 **171** 114505

Investigation of the Electrochemical Acetone Reduction Reaction in a PEM-Setup

Axel Marth,[1,2] Anna T. S. Freiberg,[1,2,*] Maximilian Maier,[1,2] Peter Wasserscheid,[1,3,4] and Simon Thiele[1,2,*,z]

[1]*Forschungszentrum Jülich GmbH, Helmholtz-Institut Erlangen-Nürnberg for Renewable Energy (IET-2), Cauerstr. 1, 91058 Erlangen, Germany*
[2]*Friedrich-Alexander-Universität Erlangen-Nürnberg, Department of Chemical and Biological Engineering, Egerlandstr. 3, 91058 Erlangen, Germany*
[3]*Forschungszentrum Jülich GmbH, Institute for a Sustainable Hydrogen Economy (INW), Brainergy Park 4, 52428 Jülich, Germany*
[4]*Friedrich-Alexander-Universität Erlangen-Nürnberg (FAU), Lehrstuhl für Chemische Reaktionstechnik (CRT), Egerlandstr. 3, 91058 Erlangen, Germany*

The electrochemical energy storage in organic compounds has gained increasing interest in recent years. The acetone reduction can serve simultaneously as a model compound for electrochemical ketone reduction and as an electrochemical liquid organic hydrogen carrier. This study investigates the influence of temperature and concentration on the electrochemical acetone reduction reaction (ARR) to isopropanol (2-propanol) in a membrane electrode assembly. It reports, in particular, on the faradaic efficiency and performance of the system both in fuel cell mode (above 0 V vs RHE) and in hydrogen pumping mode (below 0 V vs RHE). This investigation is performed by applying cyclovoltammetry, electrochemical impedance spectroscopy (EIS), and amperometry. Shape analysis of the recorded EIS data is performed, and mass transport limitation is identified as one major problem of this configuration. Additionally, thermocatalytic experiments are conducted to ensure comparability, and the specific reaction rates of both approaches are compared to each other, thus emphasizing the importance of referencing when performing electrochemical reduction experiments. Propane formation has been found as a relevant side reaction of the ARR in thermocatalytic and electrocatalytic experiments.

 [DOI: 10.1149/1945-7111/ad8d7c]

Manuscript submitted June 6, 2024; revised manuscript received October 4, 2024. Published November 12, 2024.

Supplementary material for this article is available online

Climate change forces the world economy to increase its usage of renewable energies. Due to the intermittent nature of solar and wind energy, storing energy over different periods is necessary to cover the worldwide energy demand throughout the year. While energy storage in batteries remains an option for short-term storage with many cycles throughout the year (e.g., solar energy storage over the day), decentralized seasonal energy storage remains essential. Hydrogen is assumed to be able to cover this demand.[1] Nevertheless, storing compressed hydrogen results in high investment costs for storage tanks and compressors.[2] In recent years, many research groups have taken an interest in storing hydrogen in the form of liquid organic hydrogen carriers (LOHC).[3–7] These carriers consist of a hydrogen-lean and a hydrogen-rich form. During the storage phase, the hydrogen-lean molecules are hydrogenated to their hydrogen-rich form. At the time and location of hydrogen demand, the so-obtained hydrogen-rich LOHC compounds are dehydrogenated to release the stored hydrogen. While most LOHC systems are hydrogenated/dehydrogenated through a thermal catalysis pathway, the acetone-isopropanol pair can also be used in electrochemical conversion units. The acetone hydrogenation can be performed in a proton exchange membrane (PEM) setup, sometimes called a PEM hydrogenation reactor (PEMHR) or PEM reactor.[8,9] The reactions and their electrochemical standard potentials occurring in said acetone hydrogenation are:

$$Anode\text{: } H_2 \rightarrow 2\,H^+ + 2e^-;\ E^0 = 0\ V \text{ vs. } RHE \quad [1]$$

$$Cathode\text{: } 2\,H^+ + 2\,e^- + C_3H_6O \rightarrow C_3H_8O\ ;\ E^0 = 0.118\ V \text{ vs. } RHE \quad [2]$$

$$Full\ Cell\text{: } C_3H_6O + H_2 \rightarrow C_3H_8O;\ E^0 = 0.118\ V \text{ vs. } RHE \quad [3]$$

Furthermore, the dehydrogenation can be directly coupled with an oxygen reduction reaction (ORR) in a galvanic system in form of a direct isopropanol fuel cell (DIFC) to directly convert the chemical energy to electrical energy without a hydrogen gas intermediate.[5,10] The term electrochemical liquid organic hydrogen carrier (EC-LOHC) has been introduced to differentiate this novel solution from existing LOHC technologies.[3] The advantages of electrochemical systems are manifold. They offer a high degree of automation and integration into existing technologies. They are easy to scale up and can quickly adapt to fluctuating energy excess, making them a viable option for decentralized storage solutions. In addition to its usage as a hydrogen carrier, the acetone reduction reaction (ARR) can serve as a model compound for the electrochemical reduction of simple ketones to value-added organic products. Using renewable energy to produce high-value products via electrosynthesis offers significant improvements compared to other pathways, e.g., the tailoring of selectivity as a function of the applied voltage.[9,11,12]

Nonetheless, the electrochemical reduction of organic compounds in a PEM setup is not well understood yet. Some studies investigating the electrochemical hydrogenation of acetone have been published.[13–17] Ando et al.[13] investigated the possibility of acetone hydrogenation coupled with thermal dehydrogenation of isopropanol via solar thermal energy. They examined the effects of catalyst loading, temperature, and the addition of sulfuric acid into their electrolyte in an attempt to improve proton conductivity. These authors identified the performance dependency on the cathode loading (ARR electrode), revealed an increase of performance when sulfuric acid was added, and found that higher currents can be reached when temperature increases. Other studies have also shown that increasing temperature and concentration positively impact performance.[16,18] Nevertheless, the quality of these studies

*Electrochemical Society Member.
[z]E-mail: si.thiele@fz-juelich.de

regarding a fundamental understanding of the system from an electrochemical point of view is limited and inconsistent, in particular with respect to the reported catalyst loadings, j-V characteristics, and faradaic efficiencies (FE). Furthermore, to the best of our knowledge, none of these studies used established methods like impedance spectroscopy or cyclic voltammetry to investigate and understand the ARR in a membrane electrode assembly (MEA). However, these techniques have been applied in rotating disc electrode (RDE) studies. Bondue et al.[19,20] investigated the electrochemical behavior of ketones on polycrystalline platinum in rotating ring disc electrode (RRDE) experiments[19] and performed single-crystal electrode investigations.[20] Their studies led to the conclusion that the ARR depends on the presence of certain crystal planes and that propane formation can take place as well.[20] In these RRDE experiments, fractional reaction orders for acetone were determined. This phenomenon was linked to an intermediate coverage of active species. The authors determined protonated acetone, with one proton on the ketone group, as the reactive species and concluded that a protonation of acetone in the acidic electrolyte takes place before adsorption onto the electrode.[19] This assumption complicates the adaptability of their results on MEA experiments as no liquid acidic electrolyte is present in an MEA. It is unknown if the solid electrolyte in the cathode catalyst layer would also lead to a pre-protonation of the acetone.

Our study aims to conduct a thorough electrochemical investigation of the ARR in an MEA configuration. This includes the analysis of concentration and temperature dependencies and their influence on acetone crossover, FE, and mass transport phenomena. j-V characteristics, cyclovoltammetry, electrochemical impedance spectroscopy, and product analysis (online gas chromatography for gaseous side products and offline gas chromatography for liquid products) are performed and used to determine scope and limitations of this continuous electrosynthesis approach.

Experimental

Chemicals, materials, and catalyst.—The PtRu/C catalyst with a Pt content of 40 wt% and Ru content of 20 wt% (HiSPEC 10000) and the Pt/C catalyst with a Pt content of 40 wt% (HiSPEC4000) were purchased from Alfa Aesar (USA-MA). Nafion™ D2021 and Nafion™ XL were purchased from Chemours (USA-DE). Gas Diffusion Layers (GDLs) H23C2 and H23C8 were bought from Freudenberg & Co. KG (Germany) and used for the acetone/isopropanol and hydrogen sides, respectively. Isopropanol (≥99.9%) and acetone (≥99.9%) were bought from Merck (Germany) and used without further purification. DI water, treated with a Milli-Q water purification system (18.2 MΩ, Merck, Germany), was used for ink manufacturing and cell tests. Hydrogen (≥99.999%, Air Liquide, France) was used for the electrochemical experiments.

Membrane electrode assembly manufacturing.—All electrodes were sprayed using an ExactaCoat (Sono-Tek Corporation, USA-NY). PtRu/C and Pt/C inks with a catalyst weight content of 3 wt% and 1 wt%, respectively, an ionomer content of 30 wt% of the solid content, and a water/isopropanol mixture (80/20 weight ratio) were sonicated for 25 min using an ultrasonic horn (Hielscher UP 200ST, Germany) at a power of 40 W under stirring. The inks were used to spray the electrodes with a Pt/C catalyst loading of 0.3 $mg_{Pt}\ cm^{-1}$ and a PtRu/C catalyst loading for acetone reduction of 1.0 $mg_{PtRu}\ cm^{-1}$ on the respective GDLs. The Pt/C and PtRu/C gas diffusion electrodes (GDEs) with an area of 5 cm^2 were hot-pressed onto a Nafion™ XL membrane, with an area of 25 cm^2, at 155 °C and 120 N cm^{-2} using a High-Performance Press (COLLIN Lab & Pilot Solutions GmbH, Germany) for 6 minutes.

Work station and cell setup.—The Cell Tests were performed on a custom-built test bench, including a Scribner System humidifier for the anode side (Scribner Associates Inc., USA-NC), a pressurized

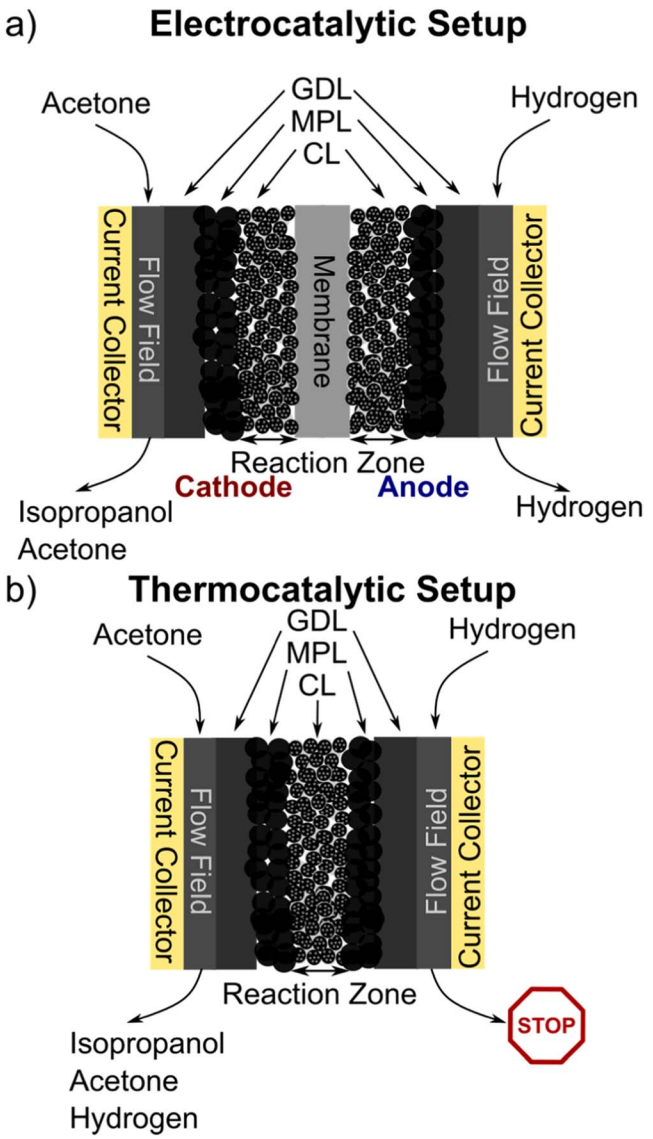

Figure 1. Cell Setup for acetone hydrogenation cell, (a) the electrocatalytic setup with flow fields, current-collectors, and membrane-electrode-assembly, consisting of gas diffusion layers (GDL) with microporous layer (MPL), catalyst layers (CL) and membrane. In (b), the thermocatalytic setup has no membrane and a dead end on the hydrogen side, thus forcing the hydrogen stream through the GDL/MPL and over the CL.

liquid container with a mass flow controller for the preheated organic reactant feed, and a VSP300 Potentiostat (BioLogic, France). A graphite single-channel multi-serpentine flow field and Scribner Fuel Cell Fixture, consisting of a hydrogen fuel cell endplate (anode) and a redox flow battery endplate (cathode) (Scribner Associates Inc., USA-NC) were used. The liquid feed was deaerated with N_2 before being filled into the pressurized liquid container for at least 15 min at 100 ml min^{-1}. Experiments were carried out at atmospheric pressure with a fixed feed rate of the reactant solution on the cathode of 7.5 ml min^{-1} and a hydrogen flow rate on the anode of 100 ml min^{-1}. The cell setup differs between the electrochemical and thermocatalytic setups. The electrocatalytic hydrogenation of acetone (Fig. 1a) is similar to the design of a proton exchange fuel cell. While an MEA is used for the electrochemical experiments, one GDE (same as the cathode in the MEA) and one GDL (same as the anode GDL) are used for the thermocatalytic experiments (Fig. 1b). Here, no membrane separates the two sides (acetone/hydrogen). Instead, hydrogen is forced through the GDL and over the CL by running into the former anode/hydrogen side dead end. A more

detailed schematic of the test station setups for the electrocatalytic and thermocatalytic experiments is portrayed in S1 and S2 in the supporting information (SI).

Analysis.—The cathode product stream was collected in a chilled three-neck round-bottom flask connected to a dimroth cooler (4 °C). One neck was connected to a nitrogen stream of 25 ml min^{-1}, serving as a carrier gas to the gas chromatograph (GC) with a TCD detector (GC; Clarus 590, PerkinElmer, Inc., USA-MA). Furthermore, the gaseous stream of the anode (hydrogen side) was sent through a chilled dimroth cooler filled with water, serving as an organic trap to determine the permeation rate. The measurement accuracy of the permeation rate is slightly diminished because the goal was to determine the permeation during the reaction. One would have to wait for a steady-state for a more precise determination. Instead, in this study the measurement of crossover started directly with the electrochemical measurement, thus not yet in steady-state. Both collected liquid products (cathode and anode side) were analyzed via headspace-GC with a flame ionization detector.

Before each experiment, an analysis of the state-of-health of the MEA was executed under blocking conditions. This state was achieved with hydrogen (100 ml min^{-1}) fed to the anode side and water fed to the cathode side. The flow of water was stopped after 15 min, and the water was deaerated electrochemically by applying a cathodic current of 10 mA cm^{-2} and waiting until the potential dropped below 0 V, thus reducing leftover oxygen in the water. Cyclovoltammetry (CV), potentiostatic electrochemical impedance spectroscopy (PEIS), crossover, and ohmic short measurements were performed to evaluate cell degradation. Afterwards, the acetone hydrogenation experiment was performed. Between experiments, the organic side was flushed with DI water to clean leftover reactants and organics to enable pristine environments after each investigation. Three different temperatures (30 °C, 50 °C, 70 °C) were investigated. For each operating temperature, three different concentrations of acetone, namely 0.25 M, 0.50 M, and 1.00 M, were fed. All tests were repeated three times with a new MEA. A simplified schematic of the performed experiments is portrayed in S3 in the SI.

Electrochemical measurements.—CVs were performed with sweep rates of 50, 75, 100, 150, and 250 mV s^{-1} starting at 0.05 V with an upper and lower vertex potential of 0.6 V and 0.0 V, respectively. The blocking-condition impedance measurements were conducted as potentiostatic electrochemical impedance spectroscopy (PEIS) at 0.2 V vs RHE with an amplitude of 3.5 mV and in a frequency range between 200 kHz and 200 mHz. The impedance data were fitted with a blocking-condition transmission line model representing the porous working electrode[21] and a pure resistor for the ohmic contributions of the membrane and electric contact, as well as an inductor for the measurement setup in series. The crossover measurement was performed by voltage stepping (0.2 V to 0.7 V in 0.1 V steps, holding time 150 s, and averaging the last 30 s). Afterward, linear regression was performed to determine the slope corresponding to R_{short}^{-1}, and the intercept representing the hydrogen crossover current.

For the hydrogenation experiments, the voltage was held for 15 min at −150, −100, −50, 0, 25, 50, 75, 100 mV and at open circuit voltage (OCV, between 120 and 150 mV). Then, PEIS was performed at the same potential from 100 kHz to 70 mHz with 10 points per decade and with perturbation between 2.5 mV and 4 mV, chosen to provide stable impedance spectra without overextending the range of perturbation, depending on the applied potential. For the 100 mV to 0 mV and the −100 mV measurement point 3.5 mV, the −150 mV point 4 mV, and the −50 mV 2.5 mV perturbation values were chosen. The −50 mV is close to the change between fuel cell mode and hydrogen pumping mode, so a smaller perturbation was decided on. The testing protocol concluded with an OCV hold for 3 min.

For comparison, hydrogen pumping experiments were conducted with the same settings and temperature as for the −50, −100, and −150 mV hydrogenation experiments. Instead of organics, deaerated water was fed into the cell at the same flow rate of 7.5 ml min^{-1}.

High-frequency resistances (HFR) were determined using an equivalent circuit (inductor + resistor) with a charge transfer transmission line model.[22] For fitting the reaction impedances (−150 mV to 100 mV), the first 36 points (100 kHz to 46.7 Hz) of each impedance spectrum were used. All impedance spectra were fitted using the impedance.py library.[23]

Thermocatalytic experiments.—For the thermocatalytic gas diffusion electrode (GDE) experiments, the same GDE as for the cathode side was used. For this, a GDE (1.0 mg_{PtRu} cm^{-1}, H23C2) and a GDL (H23C8) were placed in the cell fixture, and the former anode exhaust (blue endplate) was blocked to force the hydrogen through the GDL and over the catalyst layer. The same parameters (temperature, time, and concentration) at the same flow rate (hydrogen and acetone) as for the electrochemical experiments were chosen. The liquid and gaseous products were investigated, as explained previously.

Theory

Various faradaic and non-faradaic reactions can coincide in an electrochemical system. Determining the faradaic efficiency (FE) is relevant for investigating a specific reaction, such as the ARR. Any electrochemical reaction performs at a specific FE. This FE is the quotient of current corresponding to this reaction and absolute current and can be described as:

$$FE = \frac{j_{ARR}}{j_{absolute}} \quad [4]$$

Where FE is the faradaic efficiency, j_{ARR} and $j_{absolute}$ correspond to the current density in mA cm^{-2} of the ARR and absolute current observed.

When performing the ARR, a specific current correlating only to the acetone reduction can be determined and compared to the absolute current running through the current collectors. This is done by measuring the reaction rate of acetone conversion based on the cathode product stream analysis and calculating the correlating current density in A cm^{-2} by the following equation:

$$j_{ARR} = n \cdot v \cdot F \quad [5]$$

Where n is the number of electrons per reaction, two for the ARR, v is the reaction rate in mol s^{-1}, and F is the Faraday constant (96485 A s mol^{-1}). This way, a current breakdown of the absolute current density, ARR correlating current density, and side reaction current density is performed.

For spontaneous reactions, reactant crossover can lead to product formation without measuring a net electric current, sometimes referred to as a "chemical short." In order to only investigate the reaction rate under current, a correction is necessary. This is done by determining the reaction rate and corresponding theoretical current density at OCV for set parameters (Eq. 5) and subtracting the value from the current density under overpotential:

$$FE_{corrected} = \frac{(j_{ARR} - j_{ARR}^{OCV})}{j_{total}} \quad [6]$$

Where $FE_{corrected}$ is the corrected FE and, j_{ARR}^{OCV} is the theoretical current density under OCV. This correction is solely performed to mitigate an overestimation of FE. The origin of this reaction will be discussed later.

An increase in current, or reaction rate, can be observed with increasing overpotential. In this work, the overpotential is defined as:

$$\eta = E_{cell} - E_{OCV} \quad [7]$$

Where η is the overpotential, E_{cell} is the cell potential, and E_{OCV} is the open circuit voltage.

The reaction in an electrochemical system depends on the voltage; positive or negative overpotential can lead to an oxidative or reductive reaction on the working electrode. Furthermore, when many reactions can occur, knowing the averaged voltage at the catalyst surface is relevant. This averaged voltage differs from the measured voltage by a value correlating to the ohmic drop in a system. Therefore, we perform a voltage correction to compare different operating conditions. This voltage correction is performed by determining the high-frequency resistance of the impedance. Then, a voltage correction is achieved by following the formula:

$$E_{HFR-free} = E + j_{total} \cdot R_{HFR} \quad [8]$$

Where $E_{HFR\text{-}free}$ and E are the HFR corrected, and uncorrected voltage in V, respectively, and R_{HFR} is the area-specific high-frequency resistance in Ω cm^2.

Additionally, the influence of concentration and temperature on the reversible cell voltage can be described by the Nernst equation:

$$E_{rev} = E^0 + \frac{R \cdot T}{n \cdot F} \cdot \ln\left(\frac{a_{ox}}{a_{red}}\right) \quad [9]$$

Where E^0 is the standard potential, a_{ox} and a_{red} are the activities of oxidized and reduced species, respectively, and R is the gas constant 8.314 J K^{-1} mol^{-1}.

Furthermore, when the reactant concentration at the catalyst surface reaches zero, the resulting current density is called limiting current density. This limiting current density can be used to determine the mass transport resistance, which is defined as:

$$R_{MT} = n \cdot F \cdot \frac{\Delta c}{i_{\lim}} \quad [10]$$

Where R_{MT} is the mass transport resistance in s cm^{-1}, n is the number of electrons per reaction, F is the Faraday constant in C mol^{-1}, Δc is the concentration difference between catalyst surface (assumed to be 0) and flow field in mol cm^{-3} and i_{lim} the limiting current density in A cm^{-2}. At limiting current, a complete exhaustion of reactant at the catalyst surface is assumed, hence a concentration of 0 mol cm^{-3}. Consequently, the concentration difference is the feed concentration of acetone.

During electrosynthesis, organic compounds can permeate to the other cell compartment (e.g., cathode to anode) which leads to product loss. An optimized system should have as low as possible permeation rates, hence, an investigation and quantification of this phenomenon is necessary. The permeation rate in this study was determined in an offline measurement by washing the anode hydrogen stream in a chilled dimroth cooler. Then, the concentration of both acetone and isopropanol was determined. The following equation is used to determine the permeation rate (J in mol s^{-1} cm^{-2}):

$$J = \frac{(n_{crossover}^{organics})}{(t \cdot A)} \quad [11]$$

Where $n_{crossover}^{organics}$ is the sum of the molar amount of acetone and isopropanol in mol, t is the time of measurement in s, and A is the area of the cell, namely 5 cm^2. Furthermore, to investigate if the product or starting material makes up the majority of the permeated organics, a mole fraction $X_{Isopropanol}$ in % was determined:

$$X_{Isopropanol} = \frac{n_{Isopropanol}}{n_{crossover}^{organics}} \quad [12]$$

Where nIsopropanol is the amount of isopropanol in mol found in the crossover sample. Because on both sides a hydrogenation catalyst is used and a thermochemical reaction of hydrogen and acetone might have occurred after cross-over at the anode, this fraction does not necessarily represent the permeated isopropanol fraction but simply the isopropanol fraction measured when exiting the cell.

In general, the permeation rate can be expected to follow Fick's first law of diffusion:

$$J = -D \cdot \frac{dc}{dx} \quad [13]$$

Where J is the permeation rate mol s^{-1} cm^{-2}, D is the diffusion coefficient in cm^2 s^{-1}, c is the concentration in mol cm^{-3}, and x is the position in cm.

Results

Concentration variation.—The j-V-characteristic of the hydrogenation of a 0.25 M, 0.50 M, and 1 M acetone feed at 50 °C is shown in Fig. 2a).

The overall current densities observed are comparably small for cell potentials above 0 V (FC mode). Starting from an OCV of roughly 0.13 V, the current response upon polarization increases rapidly first. Then, it levels out into a small plateau when approaching 0 V (see inset of Fig. 2a). The current obtained during FC mode follows the trend in concentration, with the highest concentration of 1 M acetone reaching up to 200 mA cm^{-2}, whereas a feed of 0.25 M acetone only shows 72 mA cm^{-2} above 0 V. The increase of fuel cell performance with increasing feed concentration is well known and reported in the literature.[24–27] The strong dependency on the feed concentration, in combination with a limiting current response, hints towards mass transport mechanisms being the limiting factor for the acetone reduction reaction in this setup. This will be treated in depth during the EIS discussion.

Based on this observation, mass transport resistances are calculated for the last values obtained above 0 V. Filling in these values in Eq. 10 for 0.25 M, 0.50 M, and 1.00 M, mass transport resistances of 914, 1009, and 1037 s cm^{-1}, respectively, and an average value of 990∓50 s cm^{-1} are determined. These values hint at significant mass transport issues for this system, as much lower values around 1 s cm^{-1} are reported for oxygen in hydrogen-oxygen proton exchange fuel cells (PEMFCs).[28] The determination of this value is based on certain limitations. These include an unclear concentration-dependent swelling of ionomer inside the catalyst layer and the possibility that the system is not in a limiting current case as assumed for PEMFCs. Nevertheless, combined with the data presented later (see section Electrochemical Impedance Spectroscopy), we believe that mass transport issues are a relevant challenge in this system.

A closer investigation of the data below 0 V regarding mass transport resistance is not considered. This is due to the change of mass transport in hydrogen pumping (HP) mode. In a voltage range below 0 V, the hydrogen evolution reaction (HER) occurs, leading to gas bubble formation, thus changing the transport phenomena in the catalyst layer. This bubble formation changes the mass transport situation in the catalyst layer and makes a pure diffusion-based explanation obsolete.

Below 0 V, a second characteristic can be observed with an exponential current increase upon further polarization. Such an abrupt increase in current could either be a secondary ARR mechanism setting in at higher overpotential or a parasitic reaction becoming dominant at lower voltages. The HER (E^0 = 0 V vs RHE) explains the substantial increase in current in the HP mode. The rise of current in this voltage range is also reported for other PEM-setups performing hydrogenation reactions.[9]

Interestingly, the feed with the highest acetone concentration shows the lowest current response in HP mode. The control

measurement with only DI-water feed without any acetone ("0 M") leads to the highest absolute current response, supporting the hypothesis of HER also occurring in this setup. The decrease in HER current observed upon acetone addition hints toward the competing character of the HER and ARR. Reactants or intermediates of the ARR likely reduce the active catalyst sites available for the HER (see CV discussion).

Estimating the FE for the ARR at different potentials is essential as competing electrochemical reactions occur within this setup. For this, the product feed regarding the isopropanol concentration, which is the desired product of the ARR, was analyzed offline. The raw FE calculated from the measured isopropanol concentration as a function of the applied potential is plotted in Fig. 2b. The fact that the FE obtained at low overpotentials (i.e., 0.10 V cell voltage) exceeds 100% shows that a thermo-chemical formation of isopropanol occurs at relevant rates due to the crossover of the reactants. The FE was, therefore, corrected for the non-faradaic (chemical) background rate of isopropanol formation as measured at OCV (see the experimental and theory parts for details). This corrected value of the FE is shown in Fig. 2c.

Comparing the two FEs determined either with or without this correction shows that the relative extent of chemical isopropanol formation is much higher at cell potentials above 0.05 V. It becomes almost negligible at high overpotentials. However, this OCV conversion rate is too high to be negligible when comparing FEs from different operating conditions, setups, or cells. The chemical isopropanol formation rates can be calculated in terms of electric current not running through the electric circuit. This calculated "electric current" can serve as a quantity to rate the influence of chemical product formation. It can be directly compared to the current density obtained at different overpotentials and the current density assigned to the ARR calculated from the product concentration in the exhaust. For example, at OCV, the product analysis of the 50 °C, 0.50 M experiment showed a reaction rate that would correlate to a theoretical current density of 10 mA cm^{-2}: This current density is significant relative to the current densities measured at low overpotentials (17 mA cm^{-2} at 0.1 V), but becomes less substantial as overpotential increases (96 mA cm^{-2} at 0 V).

The origin of the OCV conversion rate is not fully understood yet. We assume the measured rate stems from the thermocatalytic reaction of hydrogen and acetone at the catalyst surface without current. This can occur when either molecular hydrogen or acetone cross over the membrane. For example, the hydrogen crossover hydrogenates the acetone on the cathode catalyst surface. Alternatively, the acetone crossover is hydrogenated to isopropanol on the anode catalyst surface. The isopropanol product can diffuse back to the cathode or get washed out by the gas flow in the anode compartment. Using other composite membranes or thicker membranes could decrease the effect of this OCV conversion by providing an improved permeation barrier in future works. This effect has been reported for methanol fuel cells (DMFCs).[29,30] Thicker membranes or composite membranes would likely lead to increased ohmic resistance and a performance decrease, so a trade-off between ohmic resistance and permeability has to be found. An unwanted thermocatalytical hydrogenation to isopropanol would represent a loss from an electrochemical point of view. Nevertheless, it would not be lost from a system point of view. Only if unwanted side reactions occur will the selectivity of the conversion be affected negatively. Fuel loss through the membrane could become a significant issue for a fully reversible system, such as an EC-LOHC system. The permeation of value-added products and starting material to the other side of the cell negatively affects the overall performance. Moreover, a collection pathway on the gas side is necessary to ensure no organic reactant is lost from the system.

To enable better comparability in this study and with other studies, only the corrected FE will be discussed. The corrected FE for the ARR is almost constant above 0 V cell potential, with a maximum of roughly 70% for all acetone concentrations

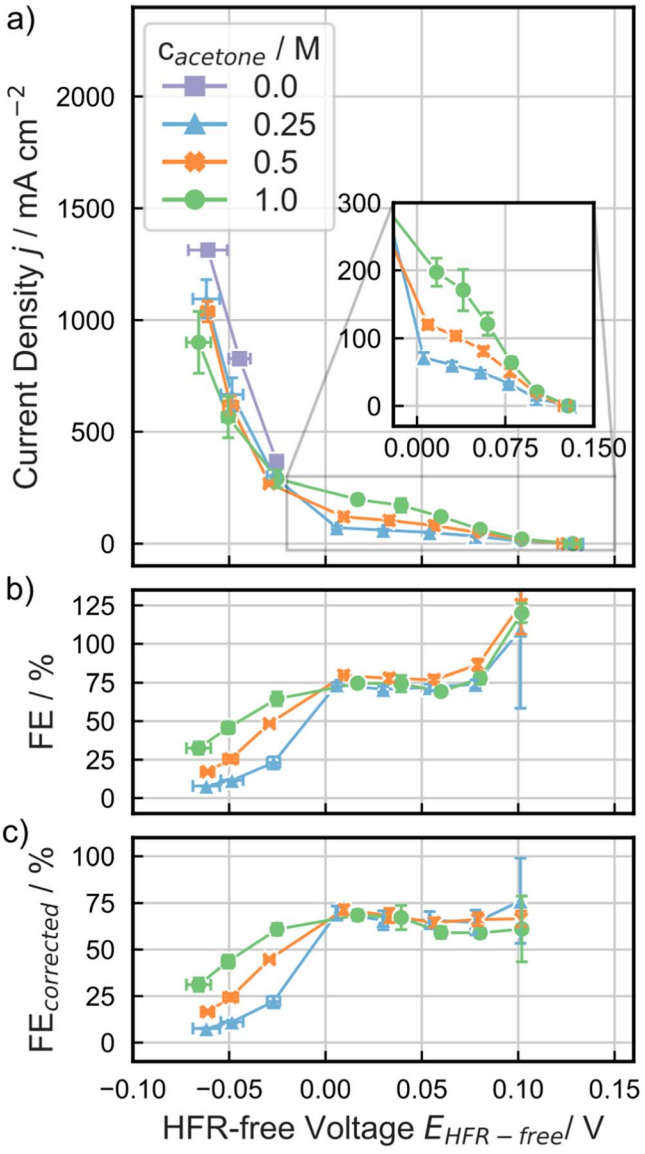

Figure 2. j-V Characteristic in dependency on HFR-corrected cell voltage (a), the corresponding uncorrected (b), and corrected (c) faradaic efficiencies at 50 °C and varying acetone concentrations of 0.25 M, 0.50 M, and 1.00 M. For comparison, the hydrogen pumping performance with a pure DI water feed on the cathode is shown in panel (a). Error bars are based on repeated measurements.

(see Fig. 2c). The current density depends on the acetone's surface coverage or availability in the FC mode (see Fig. 2a). Only a current corresponding to the acetone-covered surface can be drawn in FC mode. In FC mode this leads to a stable FE independent of voltage changes and a conversion rate solely related to the overpotential and acetone availability. Below 0 V, the vast increase in current, which was assigned to HER based on the overall current response characteristics, aligns with a rapid decrease in FE for ARR, as expected. The electrochemical acetone conversion drops faster with increasing overpotential for lower acetone concentration. This behavior would fit a competing adsorption of the ARR and HER reaction intermediates on the catalyst active sites. The competitive adsorption of acetone and hydrogen is reported for the thermocatalytic and electrocatalytic hydrogenation of acetone.[19,31] This is further supported by higher FEs observed in HP mode for higher concentrations. While in FC mode, it is likely that the ARR takes place electrochemically, it is unclear in HP mode (cell voltage < 0 V) if the acetone reduction occurs electrochemically or via a

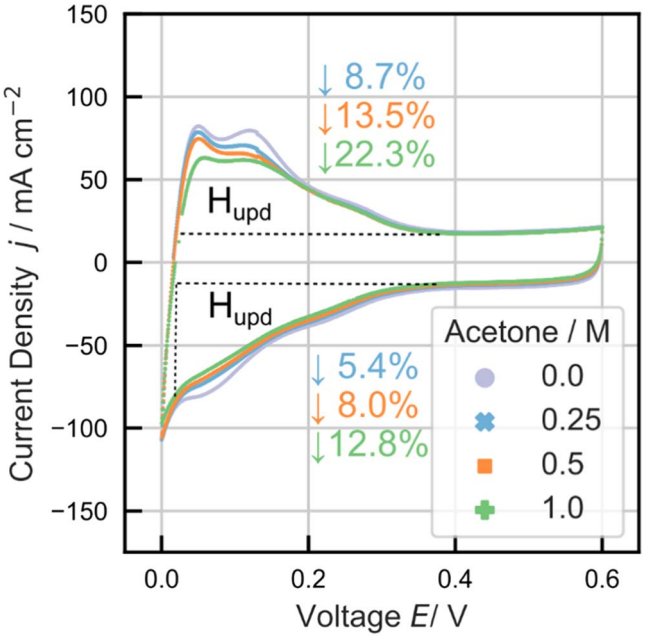

Figure 3. Cyclovoltammograms for a sweep rate of 250 mV s^{-1} at 30 °C and varying concentrations. Annotations show the relative loss of hydrogen desorption charge compared to a pure water sample.

thermal catalysis pathway due to excess hydrogen. In general, we contribute the increased FE for higher concentrations to an increased surface coverage of the catalyst layer. This increase in surface coverage would accelerate both the thermal and electrochemical reaction pathways.

Next to the acetone reduction, other side products (hydrogen and propane) occur during the process, leading to FEs below 100%. The side reactions appear to occur as a byproduct of the acetone-induced electrochemical response and include the HER and the propane formation, which was proven by online GC measurements. Propane is likely formed in a sequence of isopropanol dehydration and propene hydrogenation. However, as the setup could not quantify gaseous products, we refrain from quantifying the side reactions happening. These side products are the reason for the significantly reduced ARR FE over the whole potential range. While the HER is an electrochemical reaction, it is unclear if the propane formation takes place purely thermocatalytically or partially electrochemically, as proposed by Bondue et al.[20] A short discussion of the side products is given later in this study (see results Temperature Variation).

The results from the hydrogenation experiments hint toward competing adsorption of reaction intermediates of the ARR and HER. We, therefore, conducted CVs at 30 °C to look at the effect of different acetone concentrations on the surface adsorption charge, as shown in Fig. 3.

With increasing concentration, the hydrogen underpotential deposition (Hupd) charge decreases. This decrease can be correlated to the coverage of the catalyst with organic compounds, leading to a decrease in the available catalyst surface for hydrogen adsorption and desorption in the underpotential region. For the desorption feature, a decline in charge, compared to pure water, of 8.7%, 13.5%, and 22.3% can be seen for 0.25 M, 0.50 M, and 1.00 M, respectively. Although less distinct due to the lack of features on the PtRu catalyst, the adsorption charge changes accordingly with decreases of 5.4, 8.0, and 12.8% for 0.25 M, 0.50 M, and 1.00 M, respectively. This difference is likely correlated to the ARR's reductive current, which partially diminishes the oxidative feature (hydrogen desorption). The influence of the ARR's reductive current especially becomes more pronounced at higher concentrations. To prevent an unwanted inclusion of the HER for the adsorption charge

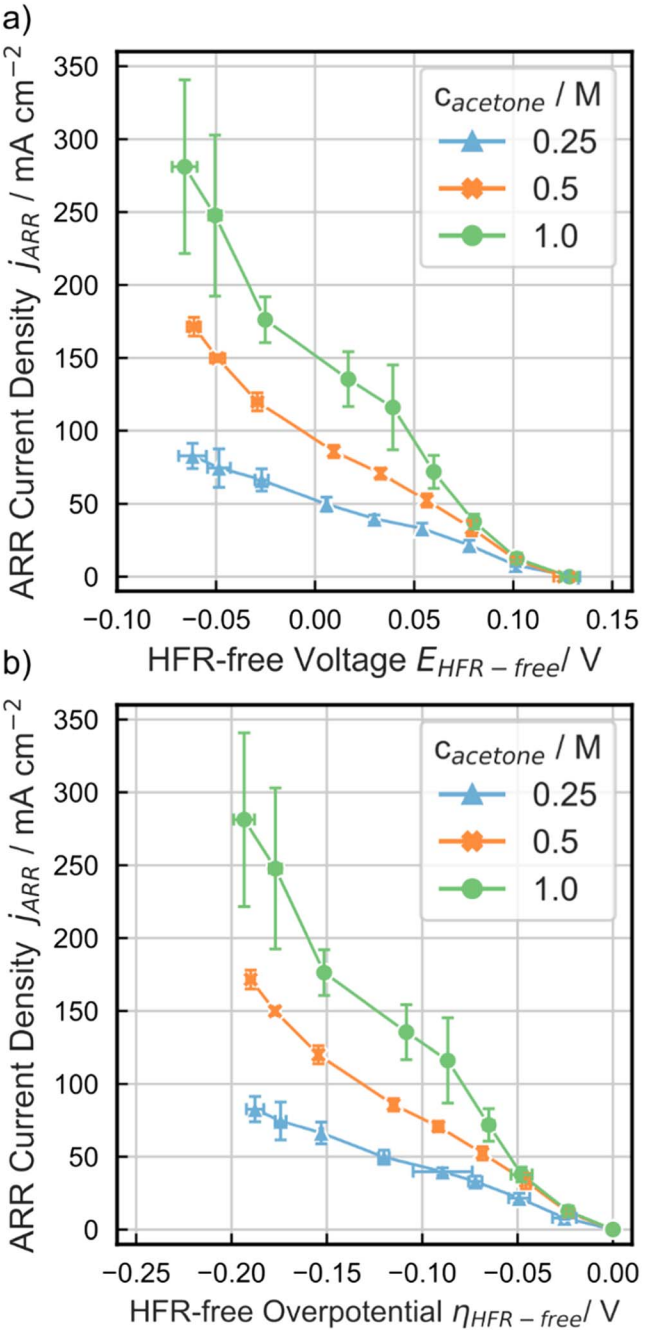

Figure 4. Current density of the acetone reduction at 50 °C and varying concentrations in dependency of HFR-corrected voltage and overpotential demonstrate the overpotential's effect on the reaction rate.

determination, the lower voltage range for integration was chosen to be 0.02 V. This voltage range is similar to the one selected for the desorption charge determination (H_{upd} area is highlighted in Fig. 3). The oxidation of hydrogen crossover can explain the general slight oxidative shift of the CV.

Combining the overall current response of the system during the hydrogenation reaction with the corrected FE (see Figs. 2a and 2c), the pure current corresponding to the ARR, jARR, and its dependency on overpotential and HFR-free voltage can be obtained. An improvement of acetone conversion with increasing overpotential can be observed (Fig. 4) despite the competing HER at low voltages.

This increase can be due to two reasons: (i) the elevated overpotential driving the improved electrochemical reaction and (ii) the thermal catalytic reaction of acetone with hydrogen in the

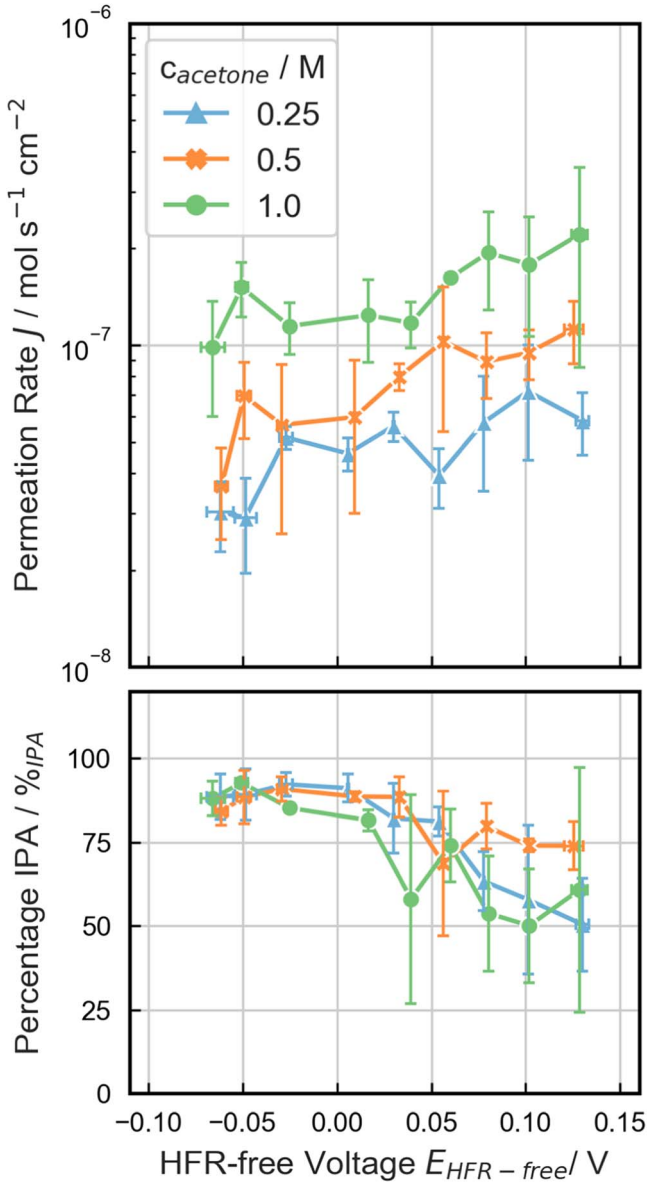

Figure 5. Organic permeation rate and fraction of isopropanol in the crossover stream for a temperature of 50 °C at varying acetone concentrations.

cathode catalyst layer (see Comparison to other hydrogenation routes). Theoretically, this thermocatalytic reaction would greatly benefit from a partial HER reaction, as H_{ads} is necessary for a Langmuir-Hinshelwood reaction pathway often discussed for thermal hydrogenation and acetone hydrogenation on platinum surfaces.[31–33] This would be a partial electrochemical reaction as the HER occurs due to the potential gradient between the anode and cathode. H_{ads} is an intermediate for the HER when assuming Volmer-Heyrovský- or Volmer-Tafel-hydrogen evolution pathways. The increased concentration-dependent conversion is linked to the increased surface coverage of the catalyst active sites with acetone (see Fig. 3) and the improved mass transport due to the concentration gradient between the surface and flow field. The reported hydrogenation-related current densities in this study are significantly higher than in other studies for electrochemical hydrogenation experiments.[9,13–16,27] The comparably large error of the 1 M sample at large overpotentials, can be correlated to an increasingly uncontrolled situation (bubble formation, simultaneous electrochemical and thermocatalytic hydrogenation) at these potentials. The bubble formation leads to a changed mass transport in the GDE, while the higher acetone concentration increases the surface coverage on the catalyst, the diffusion-based mass transport, and the thermocatalytic, and electrochemical acetone hydrogenation rates.

The concentration dependency of the mass transport is also reflected in the organic crossover (Fig. 5a).

The absolute permeation rate (isopropanol and acetone) follows the expected diffusion physics. The 0.25 M, 0.50 M and 1.00 M samples show a permeation of 5.8×10^{-8}, 1.1×10^{-7}, and 2.1×10^{-7} mol s^{-1} cm^{-2} (Fig. 5a), respectively. For this data set, the relation between permeation and concentration follows Fick's law (Eq. 13) remarkably closely. The organic compounds involved in the crossover are mostly isopropanol (Fig. 5b) for the 0.25 M and 0.50 M cases in FC mode. For the 1 M acetone experiments, the errors in isopropanol fraction are significantly higher in the FC mode and lower in the HP mode. We explain this observation due to different amounts of acetone crossing over at varying concentrations, as expected from Fick's first law. The acetone crossover might react in a less controlled fashion on the catalyst on the anode side, leading to high fluctuations in the fraction of isopropanol. Compared to high concentrations, the acetone crossover amount is lower for lower concentrations, leading to smaller fluctuations. At higher overpotentials, we believe the amount of isopropanol is higher close to the membrane, leading to mostly isopropanol crossing over. The small amount of acetone crossing over is further hydrogenated on the anode catalyst layer. An increase in error with a rise in concentration can be seen for the fraction of isopropanol (Fig. 5b). We connect this to an imperfect testing protocol. The focus of the study was the investigation of ARR-FE and not the investigation of permeation. This is why the data was recorded simultaneously with the reaction experiment to enable a correlation. Due to the previously explained reaction of acetone to isopropanol at OCV, we started every investigation with a freshly water-flushed cell. Then, the organic feed was initiated. Thus, no steady-state of permeation was established before sampling. Experiments solely focused on permeation are needed to investigate and understand the cell processes entirely.

Generally, a decrease in reversible cell voltage can be expected for increasing reactant crossover.[34] No significant shift in reversible cell voltage can be observed for the concentration variation despite the elevated permeation rates with increasing concentration (see Fig. 5). This could indicate that the chemical short due to hydrogen crossover plays a more relevant part in the change of reversible cell voltage, at least at the concentrations investigated in this study.

Temperature variation.—The influence of temperature on the ARR is displayed in Fig. 6 together with the influence of the described correction of the FE. The overall characteristics of the hydrogenation experiment follow the same behavior as shown in Fig. 2.

The overall current densities observed were small for cell potentials above 0 V (FC mode). In contrast to the increase in concentration, where no decrease in OCV was observed, a reduction in OCV can be seen for increasing temperatures. The OCV decreased from 0.137 V (30 °C) to 0.125 V (50 °C) and 0.115 V (70 °C). This decrease in OCV can be explained by a shifting Erev based on the Nernst equation (Eq. 9), its temperature dependency, and an increased crossover (both from hydrogen and organics) at elevated temperatures. Hydrogen crossover currents of 0.6, 1.0, and 1.3 mA cm^{-2} were measured for the investigated cells in oxygen-free water at 30, 50, and 70 °C, respectively. The two crossover species lead to mixed potentials on both electrodes, thus decreasing reversible cell voltage, as reported in the literature for other systems. For the DMFC the decrease in OCV with an increase in methanol crossover is documented.[35]

The current response in FC mode follows the same trend and reasoning as for the concentration variation. In general, an increase in overpotential leads to the rise of current response. Furthermore,

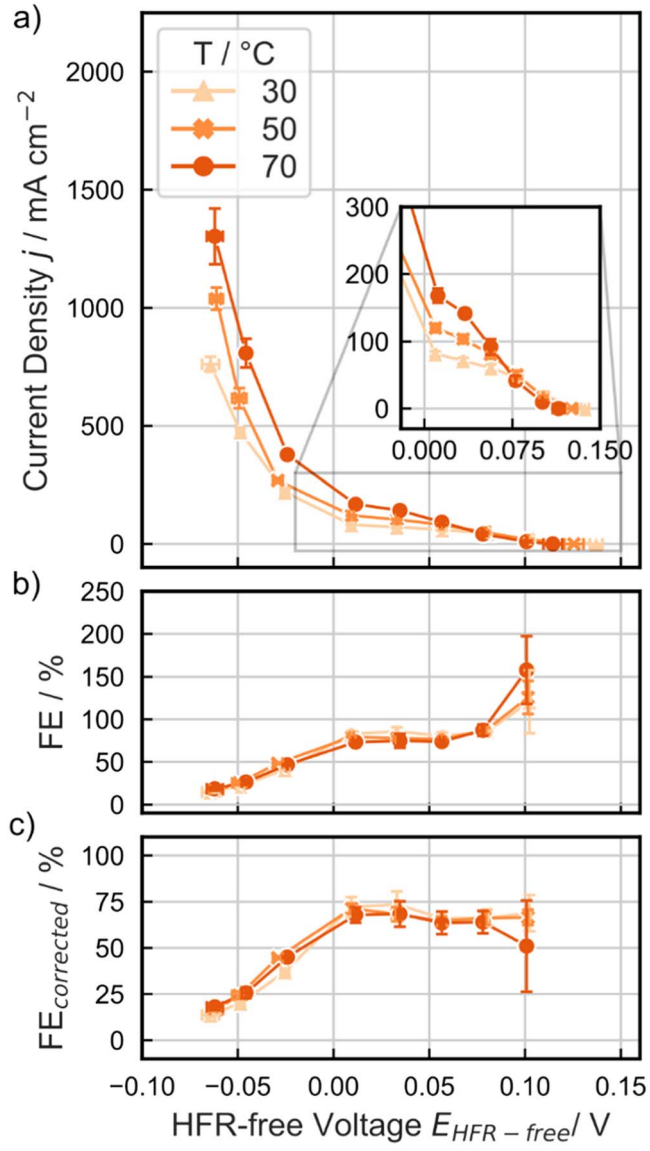

Figure 6. j-V characteristic in dependency of HFR-corrected cell voltage and the corresponding uncorrected and corrected faradaic efficiencies at 30, 50, and 70 °C at an acetone feed concentration of 0.50 M.

the increasing temperature leads to an overall increase in current. In the voltage region below 0 V, a sharp rise in current can be observed. This rise can be correlated to the HER taking place.

For values above 0 V, the corrected FE remains relatively stable, with values between 64% and 74% (Fig. 6c). When entering the HP mode, the values range between 37% (30 °C) and 45% (50 °C and 70 °C) at −50 mV and decrease and level out to 13.6%, 16.5% and 18.5% at −150 mV for 30 °C, 50 °C, and 70 °C, respectively. As previously discussed, it is unclear if the ARR occurs purely electrochemically and to which degree hydrogen (either crossover or electrochemically provided) leads to a thermocatalytic reduction of acetone. The independence of the FE from the applied temperature in FC mode hints towards the reaction taking place electrochemically. The slight dependency in the HP mode could hint towards the thermocatalytic hydrogenation of acetone making up the more significant part below 0 V. In that case, the measured current below 0 V would be mostly HP-related. This hydrogen then reacts to isopropanol with the present acetone in a thermocatalytic (non-faradaic) reaction; thus, any determined FE for the ARR below 0 V has to be looked at critically. Based on Arrhenius law, one would expect substantially higher FEs for increased temperatures in HP

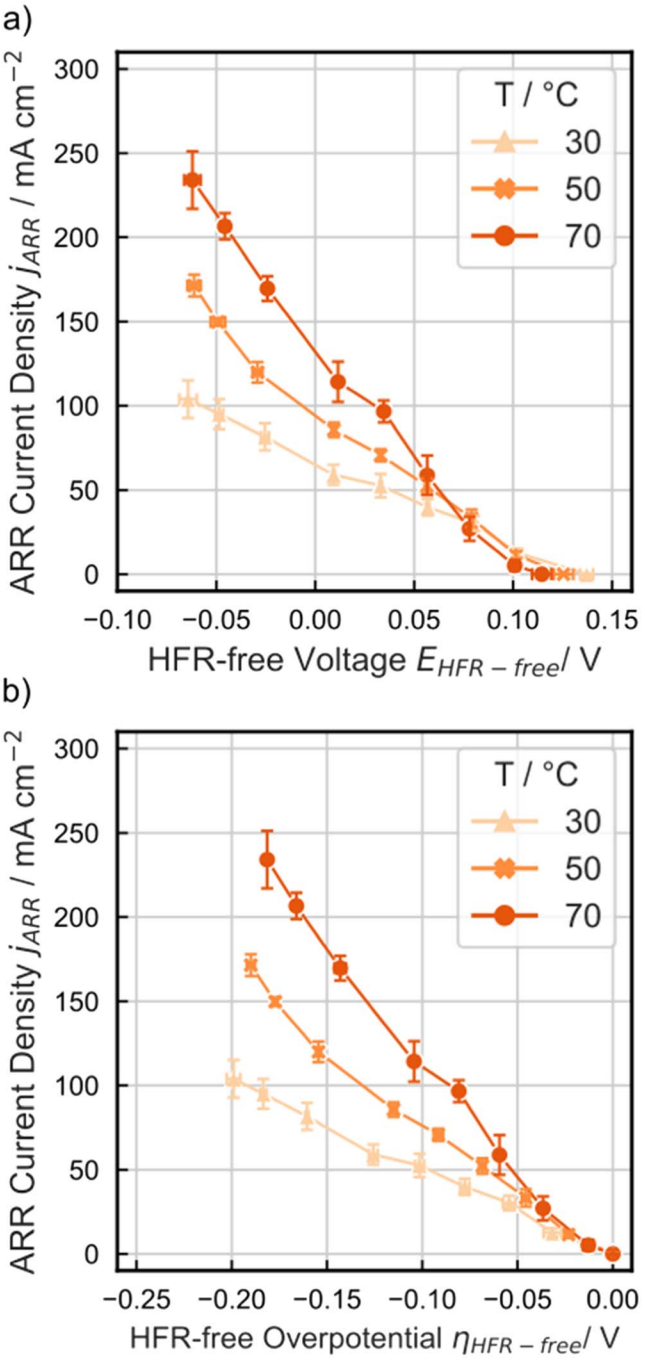

Figure 7. Current density of the acetone reduction at different temperatures in dependency on HFR-corrected voltage and overpotential, demonstrating the effect of overpotential on the reaction rate.

mode. This inconsistency could have four different origins. (i) the competitive adsorption of hydrogen and acetone. An increase in current leads to a rise in hydrogen coverage due to the HER (see Fig. 6a). This increase in hydrogen coverage would lead to a decrease in acetone coverage, making not the kinetic but the concentration of acetone the limiting factor. This hypothesis is supported by the concentration variation experiments at all investigated temperatures (30, 50, and 70 °C), where an increase in FE with an increase in concentration is observed (see SI and Fig. 2c). Furthermore, the competitive adsorption of hydrogen and acetone is reported in the literature.[31] (ii) the equilibrium shift of the reaction towards the reactant due to the exergonic nature of the reaction, which could lead to a deviation from Arrhenius's behavior. (iii) as

discussed, the system is in a diffusion-limited regime, leading to non-Arrhenius law-correlated behavior.[36] (iv) An onsetting thermal dehydrogenation of isopropanol to acetone could decrease the observed FE. This reaction would favor an increase in temperature due to its endergonic nature.[37,38]

A clear distinction between these competing reactions (thermocatalytic and electrocatalytic acetone reduction) can not be drawn based on this data set, and further experiments are needed. Nevertheless, the extent of a solely thermocatalytic acetone hydrogenation with the same catalyst layer can be determined. For this purpose, experiments with the cathode GDE were conducted and will be discussed later (see Comparison of Hydrogenation Routes).

Online GC measurements were performed to investigate gaseous side products produced in this setup. The formation of propane is proven by online GC measurement for all acetone hydrogenation experiments in this study. Furthermore, due to the HER, hydrogen is a side product of the reaction. It is unclear if the propane formation is taking place electrochemically, as proposed by Bondue et al.,[20] who investigated the electrochemical system in a single crystal setup with online mass spectroscopy, or by a thermal catalytic pathway, as reported by Sen et al.,[31] who investigated different metal-support interactions of Pt in thermal catalysis. Furthermore, it is unclear if the propane formation's starting material is isopropanol or acetone. Experiments with isopropanol feed in the voltage range below 0 V were conducted, and propane was shown as a product. Additionally, thermal catalytic experiments (see Fig. 1b) with an acetone and hydrogen feed showed the presence of propane and isopropanol. From a chemical point of view, the most likely sequence for propane formation is isopropanol dehydration to propylene followed by hydrogenation to propane. Nevertheless, Bondue et al.[20] proposed an electrochemical mechanism for the formation of propane via a partially hydrogenated acetone followed by a C–O scission to propylene and subsequent hydrogenation to propane. Based on our results, whether propane formation occurs electrochemically or by a thermal catalytic pathway is unclear. A combination of both paths is also possible. As long as hydrogen is produced as a side product, and a thermal catalysis pathway of acetone via isopropanol and propylene to propane can occur on the utilized catalyst, it is likely that a thermocatalytic propane formation also takes place in the electrochemical cell. Further investigations solely focusing on the propane reaction mechanism are necessary to understand this side reaction to a full extent. These simple experiments already show the high relevance of comparison experiments with a purely thermocatalytic setup for interpreting electrochemical hydrogenation experiments.

Through the combination of the results in Fig. 6, the dependency of the ARR on temperature is evident (Fig. 7). Higher current densities for lower temperatures can be observed for the voltage range between 0.075 and 0.14 V. For voltages below 0.075 V, the current density sharply increases with elevated temperatures (Fig. 7a). This is based on the decreased OCV due to higher reactant crossover at higher temperatures. This decrease leads to lower overpotentials at fixed absolute cell potentials, thus reducing the reaction rate. The HFR-free overpotential is shown in Fig. 7b. Here, the rise in temperature leads to an increase in reaction rate/current density for the acetone reduction in the inspected voltage region. This observation can be traced back to improved mass transport at higher temperatures and elevated kinetics. An increase in acetone reduction at elevated temperatures has been reported in the literature.[16]

The results for the temperature variation regarding organic crossover are presented in Figure 8.

In general, an increase in permeation rate with temperature is observed (Fig. 8a). The values range from 4.86×10^{-8} (30 °C) to 1.84×10^{-7} (70 °C) mol s^{-1} cm^{-2} at OCV. We contribute this to a temperature dependency of the diffusion coefficient and increased swelling at elevated temperatures, increasing mass transport through the membrane. Furthermore, isopropanol is the more considerable fraction of permeated organic compounds (Fig. 8b). The reasoning

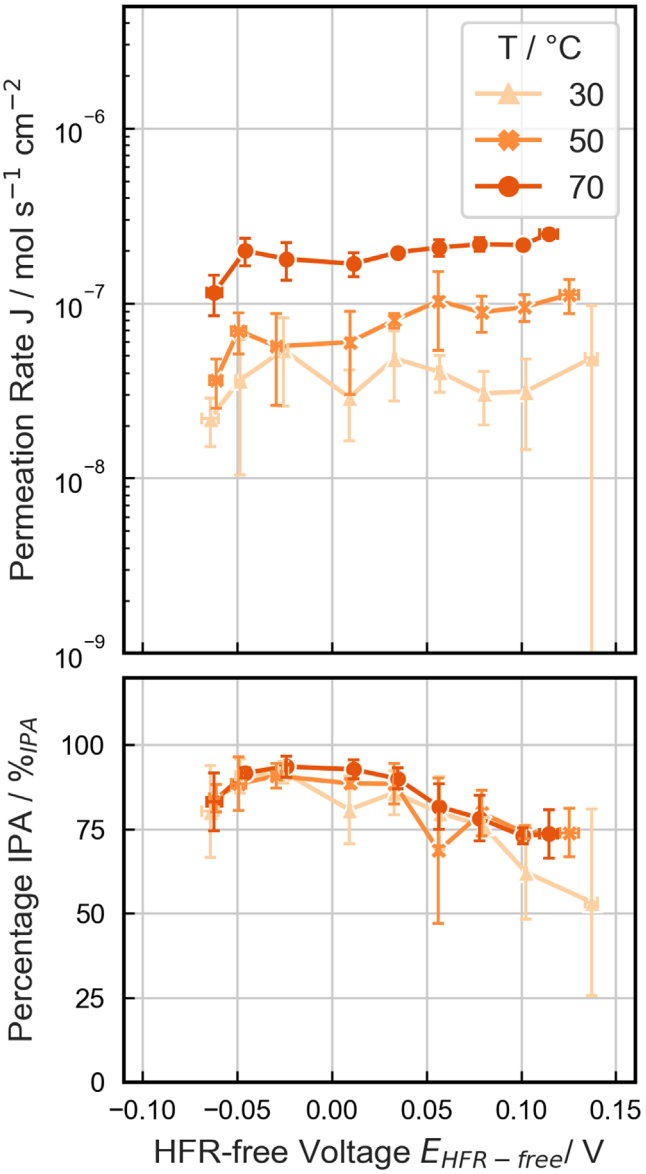

Figure 8. Organic permeation rate and fraction of isopropanol in the crossover stream for temperature variation at a concentration of 0.50 M acetone.

for the increased fraction of isopropanol in the permeated organic compounds is the same as for the concentration variation (Fig. 5b). In summary, the increase in temperature leads to a rise in current density (Fig. 6a), in reaction rate (Fig. 7), and in permeation rate (Fig. 8) due to improved mass transport.

Electrochemical impedance spectroscopy.—Based on the temperature and concentration variation results, we assume that mass transport limitations are dominating performance in the voltage range above 0 V. In contrast to DMFCs, where a liquid is fed, and a gaseous product (CO_2) diffuses out of the catalyst layer, the here-discussed system has a liquid starting material (acetone) and a liquid product (isopropanol). This leads to significant mass transport limitations. Impedance spectra were recorded to investigate this further. The 50 °C and 0.50 M parameters were chosen to compare the influence of voltage between 0.1 V and 0 V (Figs. 9a and 9b).

The measurement starts at a high frequency with an induction part (positive Im(Z)) and shows the high-frequency resistance (HFR) at around 3057 Hz and a change of slope at 74 Hz. This behavior is the same for all spectra displayed. The 50, 75, and 100 mV spectra

show parts of the transmission line model (TLM) semi-circle characteristic. With an increasing overpotential, the semicircle decreases in diameter. The 50 mV spectra show a shift in shape from an RC element between the frequencies of 1.43 and 0.9 Hz. The 25 and 0 mV spectra do not show the shape of an RC element. After the 74 Hz slope change, an impedance increase can be observed. The first decrease in semicircle diameter (100–50 mV) shows an increasing shape change depending on the applied overpotential. This is likely correlated to the decreasing charge transfer resistance at higher overpotentials. The following shift in shape can be attributed to the previously explained mass transport problem of the acetone reduction in a porous electrode, leading to diffusion limitation. A similar shape is also reported for direct methanol fuel cells when the anode side is over-compressed, leading to mass transport problems.[39]

This claim is further supported by the two-parameter variations (temperature and concentration). Figure 9d shows the concentration variation at a fixed temperature (50 °C) and a potential of 25 mV. For this variation, the 0.25 M acetone spectrum shows the steepest shape with decreasing steepness at increasing concentration. This further hints to the discussed mass transport limitation and its mitigation by increasing the feed concentration. This decrease in mass transport limitation leads to a visible semi-circle feature associated with a charge transfer reaction for the 1.00 M experiment-Furthermore, a shift of slope is observed around 0.9 Hz, indicating a mass transport limited regime. In general, an increase in HFR with an increase in concentration is discernible. The conductivity of Nafion^{TM} membranes is correlated with their humidification and water fraction. An increase in organic concentration leads to a rise in HFR. The organics take up space that is otherwise occupied by water, leading to decreased conductivity, which is known from other organic systems utilizing Nafion^{TM} membranes.[40] In Fig. 9c, the temperature variation at a fixed concentration of 0.50 M and a fixed potential of 25 mV shows that the slope after a frequency of 74 Hz becomes less steep as temperature increases. This indicates a less severe mass transport limitation. Furthermore, a higher HFR can be observed for lower temperatures. The reduction in HFR with an increase in temperature can be correlated to the rise in conductivity for PEM systems with increasing temperatures.[40,41] The combination of the results of varying overpotential (Figs. 9a and 9b), temperature (Fig. 9c), and concentration (Fig. 9d) is evidence for mass-transport-associated limitations in the herein-reported configuration.

For the investigation of the difference between the FC mode and the HP mode, as discussed in the previous section, it is relevant to look at the impedance spectra in the HP mode as well. Hence, a comparison between ARR below 0 V at 50 °C and 0.50 M (Fig. 10a) and the hydrogen pumping (pure DI water feed) is given in Fig. 10b.

For voltages below 0 V in the ARR experiments (Fig. 10a), the magnitude of impedance and the shapes of the spectra change significantly. The feature resembles a combination of two overlapping RC elements, leading to a distorted shape. The apex of impedance is for −50, −100, and −150 mV at 9.2, 2.9, and 1.8 Hz, respectively. The diameter decreases with increasing overpotential. This behavior can be linked with the steep increase in current density in this voltage range. The HER can occur at these potentials, as seen in the decreasing FE and hydrogen pumping experiments (Fig. 2a). This would correlate to a significant fraction of the catalyst layer participating in the HER reaction and, thus, a lower catalyst utilization for the ARR. This leads to a decreased RC-element,

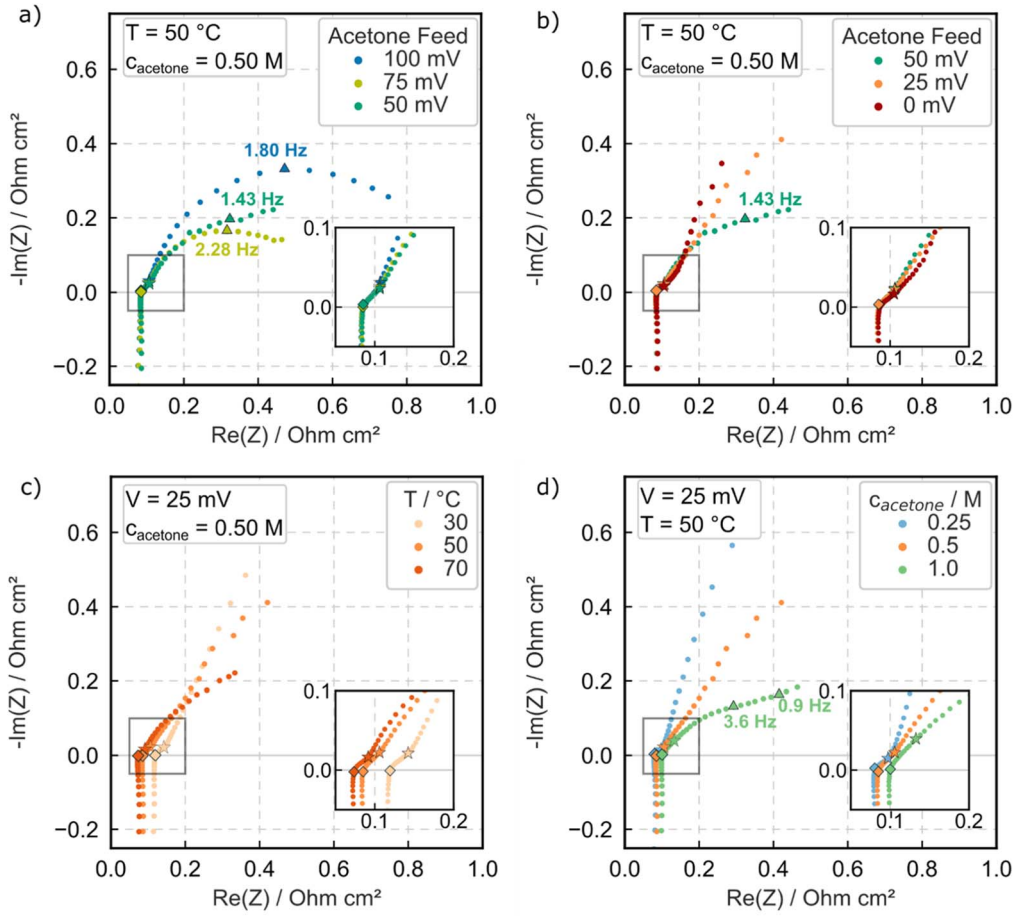

Figure 9. Impedance spectra at 50 °C and 0.50 M acetone feed at 100 mV to 50 mV (a) and 50 mV to 0 mV (b). Furthermore, impedance spectra with a 0.50 M acetone feed for varying temperatures at 25 mV (c) and at 50 °C with varying acetone concentrations at 25 mV (d). Diamonds mark the 3057 Hz frequency; stars mark a frequency of 74 Hz. Triangles mark individual frequencies, which are annotated next to the point. The last frequency point in all spectra is 0.57 Hz.

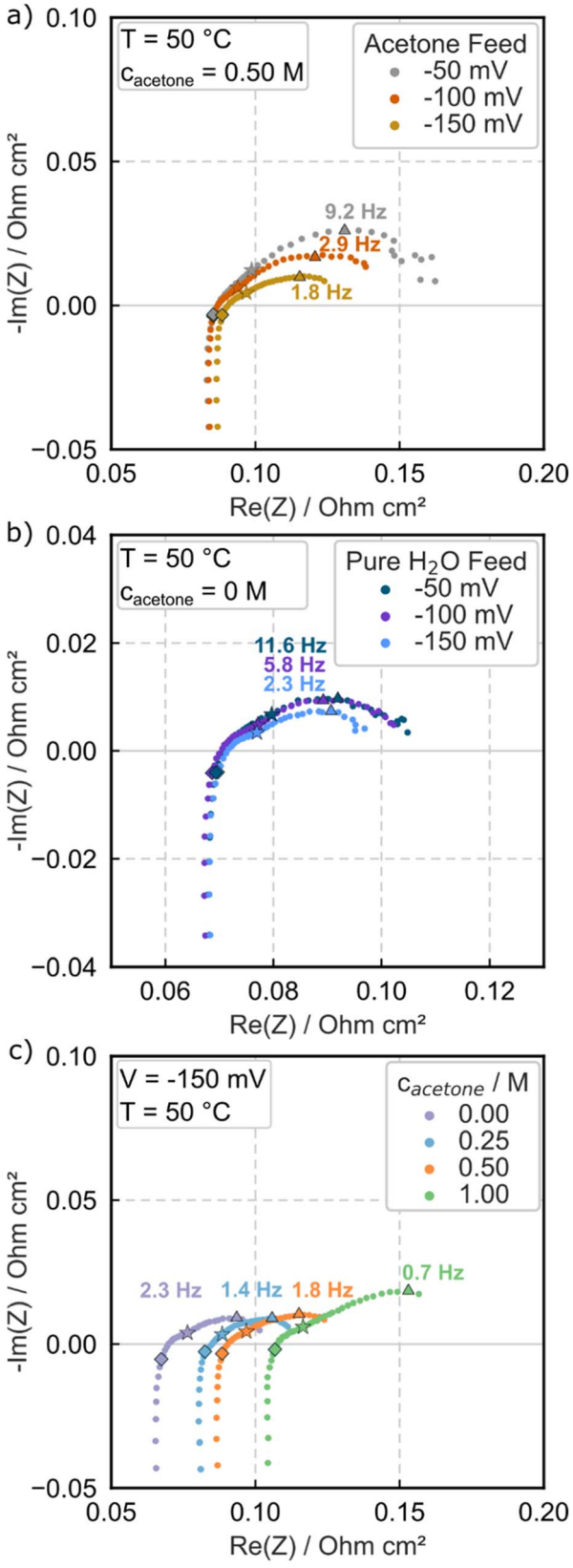

Figure 10. Comparison of impedance spectra in the HP mode at 50 °C and 0.50 M acetone feed (a), pure water feed on the cathode side (b), and at 50 °C, a potential of −150 mV, and varying acetone concentration. Diamonds mark the 3057 Hz frequency; stars mark a frequency of 74 Hz. Triangles mark individual frequencies, and the frequency is given next to the point. The last frequency point in all spectra is 0.57 Hz.

where the "apparent" charge transfer resistance is a mixture of HER and acetone charge transfer resistance. It is possible that with increasing overpotential for the HER, a more sizable portion of the catalyst surface is utilized for HER instead of ARR or thermal catalysis of acetone, thus leading to the steadily decreasing semicircle diameter. The RC element would resemble the charge transfer resistance of an HER more and more. In total, charge transfer reactions for the herein investigated system could include the HER, ARR, and possibly the propane formation. A perfect distinguishment between the possible phenomena contributing to this feature mandates a better understanding of all the side reactions and further studies.

Impedances for a cell with a pure DI water feed instead of feeding acetone are shown in Fig. 10b). A decreased HFR in comparison to the organic-fed cell can be seen. The above-mentioned water volume fraction inside the membrane can explain this change. In the hydrogen pumping scenario, pure water is fed, thus having the highest possible humidification of the membrane. This leads to a high conductivity and, hence, a low HFR.

To further elucidate this effect, the impedance spectra at varying acetone concentrations, at a temperature of 50 °C and a potential of −150 mV, are displayed (Fig. 10c). A shift of HFR can be seen for the concentration variation and follows the same trend and explanation as the impedance spectra in Fig. 9d). Furthermore, increased distortion in the RC-semi circle shape can be observed for elevated concentrations. The increased size of the RC diameter can be correlated with the above-mentioned increased surface coverage of the catalyst by organic species during the experiment (Fig. 3), thus leading to a smaller amount of catalyst surface available for HER.

In summary, the results of the impedance investigation show the influence of temperature, concentration, and overpotential on the performance of the ARR. Mass transport limitation seems to be the system's main issue, preventing higher current densities in the FC mode (Fig. 10). Furthermore, the impedance spectra present evidence for the HER in the HP mode. We refrain from fitting the whole impedance spectra with equivalent circuit models because the system is still not well understood. One example is the simultaneous reaction of HER, ARR, and possibly propane formation. Thus, faulty information could be extracted by fitting the impedance with equivalent circuit models. This is why shape analysis was performed to elucidate the effect of operation parameters on the system to avoid overinterpreting the results.

Comparison to other hydrogenation routes.—The hydrogenation and reduction of organic molecules is a widely established method in thermal catalysis. The electrochemical routes could offer benefits compared to other routes as discussed in the introduction of this study. Nevertheless, it is not trivial to directly compare the current densities of an electrochemical cell to reaction rates in thermal reactors. Moreover, it is impossible to extract reliable turnover frequencies, which are often used in the literature for heterogeneously catalyzed thermocatalytic reactions, for alloy metals in MEA configurations. This is due to the not well-defined specific charge of said alloy metals, like the one utilized herein, PtRu. A precise active site determination is impossible in electrocatalysis without such a specific charge. This specific charge is usually determined in an RDE configuration for a perfectly polished polycrystalline disc. In this study, we have decided to display the reaction rate in dependency on Platinum Group Metal (PGM) content of the cathode at a voltage of 0 V. At this voltage, the cell is still in FC mode; hence, a high FE is provided, and no additional power supply is needed.

For the investigation of the thermocatalytic reaction rate, experiments that used only the cathode electrode as a catalyst in a thermocatalytic setup were performed (Fig. 1b). For these experiments aiming to obtain a rough estimate of the thermocatalytic reaction rate of acetone reduction, the catalyst layer was directly exposed to hydrogen gas at a pressure of 1 bar, and the aqueous

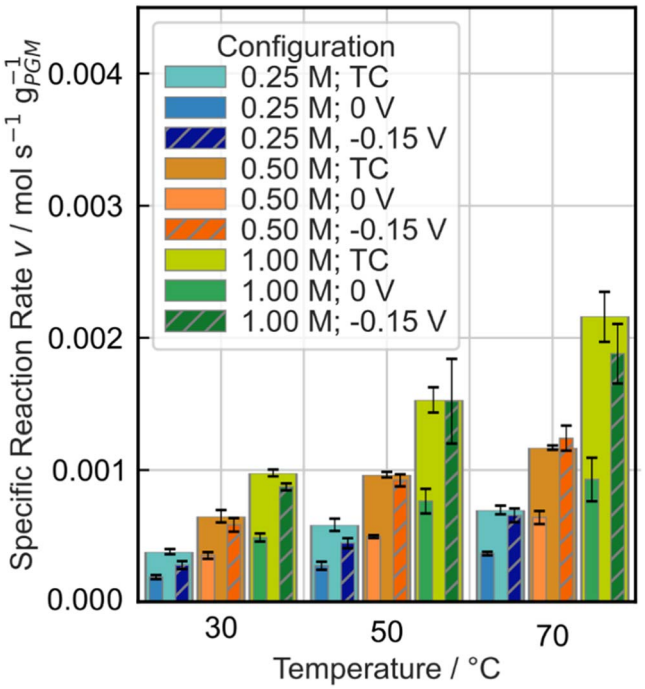

Figure 11. Comparison between thermocatalytic experiments (TC) and electrochemical experiments (EC) for the acetone reduction performed with the same GDEs at different temperatures (30 °C, 50 °C, 70 °C) and different molarities of aqueous acetone solutions (0.25 M, 0.50 M, 1.00 M). The data at 0 V and −0.15 V are given for the electrochemical experiments.

acetone solution was fed to the gas diffusion layer side of the electrode. The specific reaction rates of both the thermocatalytic and electrochemical setups are given in Fig. 11.

In general, the thermocatalytic experiments (TC) show superior results in comparison to the 0 V experiments and comparable results to the −0.15 V experiments. This indicates that the system, at its current level, is inferior to the TC setup in terms of isopropanol formation. As no investigation of the gaseous side product (propane) was performed in this study, it is possible that a higher degree of selectivity control could be achieved in the electrochemical setup. This could be especially true in the voltage range above 0 V, where a stable FE was obtained for all investigated parameters. Other groups have shown that stereoselectivity during hydrogenation can be achieved through electrocatalysis.[11] Below 0 V, the presence of molecular hydrogen on the cathode catalyst layer likely leads to a large degree of thermal catalytic formation of isopropanol. Hence, it diminishes the potential advantage of increased control over the system. This hypothesis is supported by the minuscule differences between reaction rates at −0.15 V and a pure TC pathway. The authors want to emphasize the high relevance of being cautious with values for reaction rates for an "electrochemical" hydrogenation setup at values below 0 V as it is likely that the reliability of these data is strongly influenced by a large portion of thermocatalytic reaction taking place.

Conclusions

In this study, the influence of concentration and temperature on the ARR was investigated both in a fuel cell (>0 V) and hydrogen pumping configuration (<0 V). Cyclovoltammetry, impedance spectroscopy, and constant voltage techniques were applied to elucidate limitations and to explain the observed behavior. FE corrections were performed to prevent the overestimation of experimental data.

FEs were stable throughout the experiments in the fuel cell mode. When entering the hydrogen pumping mode, the FEs were consistent for a set of temperatures but varied for the concentration variation. With an increase in concentration, the FE increased. Combined with the results presented for cyclovoltammetry, this implies a higher surface coverage of acetone, leading to this higher FE. It is unclear if this is correlated to a larger quantity of acetone being reduced electrochemically or more acetone being hydrogenated by adsorbed hydrogen after hydrogen pumping. Both effects would result in a higher FE. The thermocatalytic experiments performed in this study show reaction rates similar to those in HP mode. This could hint to a large quantity of the acetone being thermally hydrogenated, but for a clear distinction between a pure thermocatalytic pathway (reaction of H_2 and acetone on PtRu) and a partially electrochemical pathway (reaction of 2 H_{ads} and acetone on PtRu), the data give no final conclusion.

Both temperature and concentration variation showed increased permeation rates when the corresponding parameters were increased. This can be partially explained by the influence of temperature on mass transport and the influence of the concentration gradient on diffusion based on Fick's 1st law. The fraction of isopropanol was found to be highest in the crossover of organic compounds. This can be explained by acetone permeating and then being hydrogenated thermally on the platinum of the anode side or by the increased isopropanol concentration close to the membrane.

The performed impedance spectroscopy was discussed based on shape analysis and implies significant mass transport limitations governing the system. This is supported by the high R_{MT} calculated based on limiting current density in FC mode. Furthermore, the influence of temperature and organic concentration on the ohmic resistance of the system was discussed. The increase in temperature leads to a rise in conductivity, while the organic concentration leads to a decrease in conductivity.

In this study the presence of side reactions was proven and discussed. These side reactions include a thermocatalytic and/or electrocatalytic propane formation, the thermocatalytic hydrogenation of acetone to isopropanol and the electrocatalytic HER. The fraction of the individual side reaction varies depending on the applied potential, feed concentration and temperature.

This study represents a first step towards a fundamental understanding of the electrochemical acetone reduction in a PEM setup based on electrochemical analysis and techniques. Further research is needed to complete this understanding of its practical use in hydrogen storage devices based on the electrochemical conversion of the acetone/isopropanol LOHC couple.

Appendix

Supplementary Material with measurement data for all investigated concentrations (0.25, 0.50, 1.00 M) for all investigated temperatures (30, 50, 70 °C) are provided. A simplified flow chart for the electrochemical measurements, as well as a depiction of the setup for the thermocatalytic and electrocatalytic experiments, is provided in the SI.

ORCID

Axel Marth https://orcid.org/0000-0002-6720-2956
Anna T. S. Freiberg https://orcid.org/0000-0002-7885-7632
Maximilian Maier https://orcid.org/0000-0003-2698-9198
Peter Wasserscheid https://orcid.org/0000-0003-0413-9539
Simon Thiele https://orcid.org/0000-0002-4248-2752

References

1. O. Schmidt, S. Melchior, A. Hawkes, and I. Staffell, *Joule*, **3**, 81 (2019).
2. A. M. Elberry, J. Thakur, A. Santasalo-Aarnio, and M. Larmi, *Int. J. Hydrogen Energy*, **46**, 15671 (2021).
3. J. Cho, B. Kim, S. Venkateshalu, D. Y. Chung, K. Lee, and S-I. Choi, *J. Am. Chem. Soc.*, **145**, 16951 (2023).
4. A. Mehranfar, M. Izadyar, and A. A. Esmaeili, *Int. J. Hydrogen Energy*, **40**, 5797 (2015).
5. P. Hauenstein, D. Seeberger, P. Wasserscheid, and S. Thiele, *Electrochem. Commun.*, **118**, 106786 (2020).
6. K. Matsuoka, K. Miyoshi, and Y. Sato, *J. Power Sources*, **343**, 156 (2017).
7. D. Teichmann, W. Arlt, P. Wasserscheid, and R. Freymann, *Energy Environ. Sci.*, **4**, 2767 (2011).

8. A. Fukazawa, Y. Shimizu, N. Shida, and M. Atobe, *Org. Biomol. Chem.*, **19**, 7363 (2021).
9. S. Nogami, K. Nagasawa, A. Fukazawa, K. Tanaka, S. Mitsushima, and M. Atobe, *J. Electrochem. Soc.*, **167**, 155506 (2020).
10. P. Hauenstein, I. Mangoufis-Giasin, D. Seeberger, P. Wasserscheid, K. J. Mayrhofer, I. Katsounaros, and S. Thiele, *Journal of Power Sources Advances*, **10**, 100064 (2021).
11. A. Fukazawa, J. Minoshima, K. Tanaka, Y. Hashimoto, Y. Kobori, Y. Sato, and M. Atobe, *ACS Sustainable Chem. Eng.*, **7**, 11050 (2019).
12. S. Jung and E. J. Biddinger, *ACS Sustainable Chem. Eng.*, **4**, 6500 (2016).
13. Y. Ando, T. Tanaka, and M. Amano, *Energy Convers. Manage.*, **44**, 2811 (2003).
14. Y. Ando, Y. Aoyama, T. Sasaki, Y. Saito, H. Hatori, and T. Tanaka, *BCSJ*, **77**, 1855 (2004).
15. P. B. L. Chaurasia, Y. Ando, and T. Tanaka, *Int. J. Sustainable Energy*, **26**, 107 (2007).
16. S. K. Green, G. A. Tompsett, H. J. Kim, W. B. Kim, and G. W. Huber, *ChemSusChem*, **5**, 2410 (2012).
17. N. Kariya, A. Fukuoka, and M. Ichikawa, *Physical Chemistry Chemical Physics: PCCP*, **8**, 1724 (2006).
18. C. Li, A. Sallee, X. Zhang, and S. Kumar, *Energies*, **11**, 2691 (2018).
19. C. J. Bondue and M. Koper, *J. Catal.*, **369**, 302 (2019).
20. C. J. Bondue, F. Calle-Vallejo, M. C. Figueiredo, and M. T. M. Koper, *Nat. Catal.*, **2**, 243 (2019).
21. J. Landesfeind, J. Hattendorff, A. Ehrl, W. A. Wall, and H. A. Gasteiger, *J. Electrochem. Soc.*, **163**, A1373 (2016).
22. R. Makharia, M. F. Mathias, and D. R. Baker, *J. Electrochem. Soc.*, **152**, A970 (2005).
23. M. Murbach, B. Gerwe, N. Dawson-Elli, and L. Tsui, *JOSS*, **5**, 2349 (2020).
24. A. Azam, S. H. Lee, M. S. Masdar, A. M. Zainoodin, and S. K. Kamarudin, *Int. J. Hydrogen Energy*, **44**, 8566 (2019).
25. K. Scott, W. Taama, P. Argyropoulos, and K. Sundmacher, *J. Power Sources*, **83**, 204 (1999).
26. Y. Feng, H. Liu, and J. Yang, *Sci. Adv.*, **3**, e1700580 (2017).
27. X-Z. Yuan, Z-F. Ma, Q-G. He, J. Hagen, J. Drillet, and V. M. Schmidt, *Electrochem. Commun.*, **5**, 189 (2003).
28. A. Orfanidi, P. Madkikar, H. A. El-Sayed, G. S. Harzer, T. Kratky, and H. A. Gasteiger, *J. Electrochem. Soc.*, **164**, F418 (2017).
29. Z. Gaowen and Z. Zhentao, *J. Membr. Sci.*, **261**, 107 (2005).
30. Y. Wei, S. Matar, L. Shen, X. Zhang, Z. Guo, H. Zhu, and H. Liu, *Int. J. Hydrogen Energy*, **37**, 1857 (2012).
31. B. Sen, *J. Catal.*, **113**, 52 (1988).
32. A. Monteirogezork, R. Natividad, and J. Winterbottom, *Catal. Today*, **130**, 471 (2008).
33. M. J. Vincent and R. D. Gonzalez, *Appl. Catal., A*, **217**, 143 (2001).
34. R. Jiang and D. Chu, *J. Electrochem. Soc.*, **151**, A69 (2004).
35. Z. Qi and A. Kaufman, *J. Power Sources*, **110**, 177 (2002).
36. P. Castaño, J. M. Arandes, B. Pawelec, J. L. G. Fierro, A. Gutiérrez, and J. Bilbao, *Ind. Eng. Chem. Res.*, **46**, 7417 (2007).
37. Y. Ukisu and T. Miyadera, *React. Kinet. Catal. Lett.*, **81**, 305 (2004).
38. F. Xin, M. Xu, X-F. Li, and X-L. Huai, *J. Therm. Sci.*, **22**, 613 (2013).
39. G. Deng, L. Liang, C. Li, J. Ge, C. Liu, Z. Jin, and W. Xing, *J. Power Sources*, **427**, 120 (2019).
40. Y. Sone, P. Ekdunge, and D. Simonsson, *J. Electrochem. Soc.*, **143**, 1254 (1996).
41. L. Liu, W. Chen, and Y. Li, *J. Membr. Sci.*, **504**, 1 (2016).